Accepted Manuscript

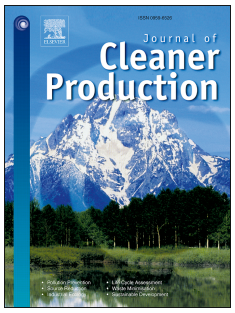

Influence of pollution control on air pollutants and the mixing state of aerosol particles during the 2nd World Internet Conference in Jiaxing, China

Lijuan Shen, Honglei Wang, Sheng Lü, Xiaohan Zhang, Jing Yuan, Shikang Tao, Guojun Zhang, Fei Wang, Li Li

PII: S0959-6526(17)30328-1

DOI: 10.1016/j.jclepro.2017.02.114

Reference: JCLP 9040

To appear in: *Journal of Cleaner Production*

Received Date: 25 October 2016

Revised Date: 8 January 2017

Accepted Date: 14 February 2017

Please cite this article as: Shen L, Wang H, Lü S, Zhang X, Yuan J, Tao S, Zhang G, Wang F, Li L, Influence of pollution control on air pollutants and the mixing state of aerosol particles during the 2nd World Internet Conference in Jiaxing, China, *Journal of Cleaner Production* (2017), doi: 10.1016/j.jclepro.2017.02.114.

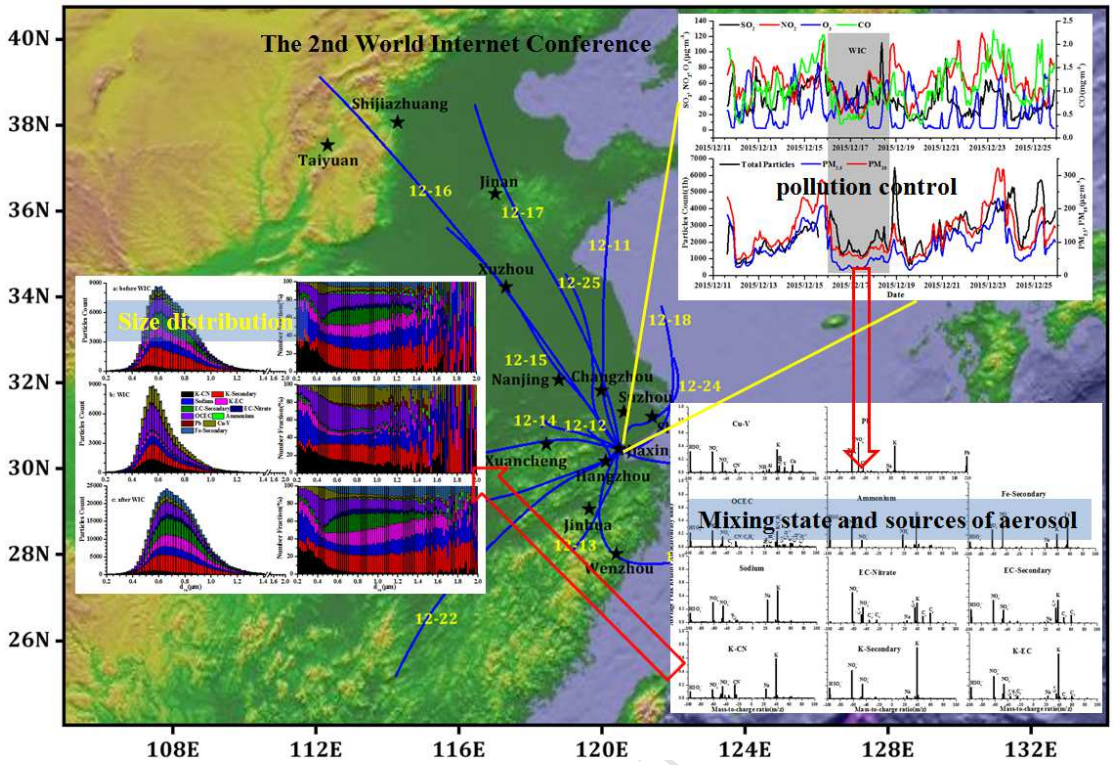

Influence of pollution control on air pollutants and the mixing state of aerosol particles during the 2nd World Internet Conference in Jiaxing, China

Lijuan Shen [a,b], Honglei Wang [c*], Sheng Lü [b], Xiaohan Zhang [b], Jing Yuan [b], Shikang Tao [d], Guojun Zhang [b], Fei Wang [b], Li Li [b]

a Jiangsu Key Laboratory of Atmospheric Environment Monitoring and Pollution Control (AEMPC), School of Environmental Sciences and Engineering, Nanjing University of Information Science &Technology, Nanjing 210044, China

b Jiaxing Environmental Monitoring Station, Jiaxing 314000, China

c Key Laboratory of Meteorological Disaster, Ministry of Education (KLME), Joint International Research Laboratory of Climate and Environment Change (ILCEC), Collaborative Innovation Center on Forecast and Evaluation of Meteorological Disasters, Key Laboratory for Aerosol-Cloud-Precipitation of China Meteorological Administration, Nanjing University of Information Science & Technology, Nanjing 210044, China

d State Environmental Protection Key Laboratory of the Cause and Prevention of Urban Complex Air Pollution, Shanghai Academy of Environmental Sciences, Shanghai 200233, China

*Corresponding author:

Phone: 0086-2558731592

E-mail: hongleiwang@nuist.edu.cn

Highlights

1. The concentrations of $PM_{2.5}$, PM_{10}, NO_2, and CO were decreased by 31.2-62.1 % during the WIC.

2. SPAMS was used to characterize more than 877,397 single particles.

3. Signals from 23$[Na]^+$ were uniformly observed among 11 types of particles.

4. The proportions of K-CN, OCEC, and Cu-V particles increased significantly during the WIC.

Abstract:

Strict pollution-control measures were implemented in Jiaxing and surrounding regions in China during the 2015 2nd World Internet Conference (WIC) to ensure good air quality. To

investigate the variations of air pollutants and the sources and mixing state of size-resolved aerosols in response to the emission controls, trace gases (O_3, SO_2, NO_2, and CO), particulate matter ($PM_{2.5}$ and PM_{10}), and single particle aerosols were measured in Jiaxing, China during December 11-25, 2015. During the WIC (from 00:00 on Dec. 16 to 16:00 on Dec. 18, 2015), the average concentrations of $PM_{2.5}$, PM_{10}, NO_2, and CO in Jiaxing were 38.7, 75.0, and 43.5 $\mu g \cdot m^{-3}$ and 0.7 $mg \cdot m^{-3}$ and were decreased by 62.1 %, 47.1 %, 31.2 %, and 41.7 % and 60.0 %, 45.7 %, 34.7 %, and 41.7 % compared to before and after the WIC, respectively. These changes were caused mainly by strict measurement of traffic restrictions and industrial emission reductions. By using the single particle aerosol mass spectrometer (SPAMS), 8,350,772 particles with aerodynamic diameters ranging from 0.2 to 2.0 μm were identified. Of these particles, 877,397 were successfully ionized. The aerosol particles collected for SPAMS data analysis employed 96.0 % of the hit particles to recognize 5 major particle classes: K-rich particles (K-CN, K-Secondary, and K-mixed Elemental Carbon (K-EC)), sodium particles, carbon-rich particles (EC-Nitrate, EC-Secondary, and Organics and Elemental Carbon (OCEC)), ammonium particles, and heavy-metal particles (Fe-Secondary, Pb, and Cu-V). Signals from 23$[Na]^+$ were uniformly observed among these 11 types of particles, which may have been affected by sea salt particles in the coastal city of Jiaxing. During the WIC, the proportions of K-EC (4.5 %), EC-Secondary (2.0 %), Fe-Secondary (1.9 %), EC-Nitrate (0.5 %), and Ammonium (0.7 %) decreased, the proportions of K-CN (15.2 %), OCEC (27.5 %), and Cu-V (16.8 %) increased significantly, and the proportions of K-Secondary (17.2 %), sodium (11.6 %), and Pb (2.0 %) changed slightly. During the WIC, the peaks representing different particle classes shifted to fine particle segments at 0.5-0.6 μm, and the peak width was relatively narrowed compared to before and after the WIC. The reduction of air pollutant emissions significantly influenced the K-CN, OCEC, Cu-V, EC-Secondary, Fe-Secondary, and K-EC particles with sizes of 0.4-1.4 μm. The information obtained on variations of air pollutants, the mixing state, and the temporal variation of particle types is essential for developing an understanding of air quality assurance control for subsequent WICs and of the origin and evolution processes of atmospheric aerosols.

Key words: 2nd World Internet Conference; mixing state; air pollutants; source; Jiaxing

1 Introduction

Atmospheric aerosols are a major component in the air and play a key role in affecting visibility, human health, and global climate change (Cao et al., 2012; Haywood et al., 1999; Kim et al., 2013). The main sources for aerosols are anthropogenic emissions, such as industrial, vehicle exhaust, and domestic emissions (Fu et al., 2008; Hildemann et al., 1991; Sun et al., 2004). Apart from emitting aerosols directly, human activities can also emit large amounts of precursor gases (such as NO_x, SO_2, CO, and VOCs), which can generate numerous secondary aerosols via the gas-particle conversion process (Kulmala et al., 2004; Zhang et al., 2010). Hence, the chemical components of urban aerosols are very complex and may determine their optical properties, hygroscopicity, residence time, and toxicological character. The secondary inorganic compositions of sulfates, nitrates, and ammonium salts may accelerate aerosol hygroscopicity (Zhu et al., 2011). Carbonaceous aerosols can enhance their light extinction efficiency (Fuller et al., 1999), and heavy metals and organic components can make aerosols more toxic (Demayo et al., 1982; Kim et al., 2013).

As one of the six largest city clusters in the world, the Yangtze River Delta (YRD) is suffering serious air pollution due to the rapid increase in emission of pollutants. In recent years, studies pertaining to the compositions, size distributions, sources, and temporal and spatial distributions of the aerosols have been widely conducted (Ding et al., 2013; Fu et al., 2008; Hu et al., 2014; Yang et al., 2012; Zhang et al., 2014). The visibility in the YRD decreased sharply from 13.2 km to 10.5 km during 1980-2000, and the fine particulate matter is responsible for the region's haze pollution (Cheng et al., 2013). Hu et al. (2014) studied that the average $PM_{2.5}$ and PM_{10} concentrations in the YRD region were reported to be 42.8 $\mu g \cdot m^{-3}$ and 74.9 $\mu g \cdot m^{-3}$, respectively, and the $PM_{2.5}$ was observed to be negatively correlated with wind speed. Information about the mixing state of individual particles is critical to understanding the hygroscopic and optical properties of aerosol particles and to providing knowledge of their atmospheric aging and reaction processes; this information serves as a bridge for combining laboratory and field experiments (Li et al., 2016; Pósfai and Buseck, 2010). Sun et al. (2013) demonstrated that primary organic aerosols (POA) were dominant during winter in Beijing, China, and that they accounted for 69.0 % of organic aerosols (OA), with the other 31.0 % being secondary organic aerosols (SOA), based on measurements from an Aerodyne Aerosol Chemical Speciation Monitor. The sources and formation mechanisms of different particle types can be determined from the

mixing state of aerosol particles (Bi et al., 2011; Dall'Osto et al., 2009; Healy et al., 2013; Moffet et al., 2008a, b; Yang et al., 2012; Zhang et al., 2013, 2014).

The Beijing 2008 Olympic Games, 2014 Asia-Pacific Economic Cooperation (APEC), and Nanjing 2014 Youth Olympic Games provided an experimental opportunity to study the impacts of emission controls on air pollution (Li et al., 2016; Sun et al., 2016; Wang et al., 2010; Wang et al., 2016; Zhou et al., 2010). During the implementation processes of control measures, primary gaseous species and particulates from vehicle emissions and coal combustion decreased significantly, while secondary pollutants increased (Sun et al., 2016; Wang et al., 2010; Zhou et al., 2010). The emission controls normally were implemented in a relatively small range of several cities and had limited influences on regional-scale secondary pollutants. In addition, meteorological conditions were found to play a more important role than emission controls in reducing PM levels (Sun et al., 2016; Wang et al., 2009). The emission controls mentioned above were mainly centralized in the inland city and in the seasons of summer or autumn with good diffusion conditions. The 2nd World Internet Conference (WIC) was held on December 16-18, 2015, in Wuzhen, Zhejiang, China. As is well known, haze pollution occurs frequently in the YRD region in winter (Kang et al., 2013). Because it is a coastal city in the YRD, the meteorological conditions in Jiaxing are more complex and mutable than those in Beijing or Nanjing. Therefore, far stricter emission controls were imposed during the WIC. During the WIC, the core area (radius of 50 km^2 from the center of Wuzhen) and the strictly controlled area (radius of 100 km^2 from the center of Wuzhen) implemented air pollution control according to the Project of Environment Quality Assurance during the Second World Internet Conference. According to the Environment Quality Assurance Scheme During the 2nd WIC published by the People's Government of Zhejiang Province, emission sources from industry, traffic, and dust were strictly controlled during the WIC. For example, pollutant emissions from power plants were decreased by 50.0 % in the core area and by 30.0 % in the strictly controlled area. The key controlled exhaust companies were shut down in the core area and asked to reduce air pollutant emissions by 30.0 % in the strictly controlled area. Construction plants were completely shut down and closed to 50 % in the core area and strictly controlled area, respectively. Straw burning and waste incineration were rigidly prohibited. Apart from domestic activity, vehicles including low-speed trucks, "yellow label" cars, and vehicles transporting dust-generating materials such as coal, muck, and gravel were forbidden

in the core area. However, how these emission controls affect the chemical composition, mixing state, sources, and formation mechanisms of aerosol particles under variable meteorological conditions remains poorly understood.

This study was carried out at the Jiaxing Environmental Monitoring Station, 20 km from the conference center. Trace gases (O_3, SO_2, NO_2, and CO), PM ($PM_{2.5}$ and PM_{10}), and the aerosol mixing state were measured simultaneously from December 11-25, 2015, by using the EMS system, Sharp 5030, and SPAMS. We analyzed the variation characteristics of air pollutants and the impacts of emission controls on pollutants during the WIC. Additionally, the influences of air masses and emission sources on air pollutants were examined by using the HYSPLIT model and MEIC data. Furthermore, the chemical compositions and size distributions of aerosols during the WIC were investigated intensively. During the WIC, 8,350,772 particles were successfully ionized and then divided into 11 types of aerosol particles. The mixing state and sources of these 11 aerosol types were then considered in detail. As the permanent venue for the World Internet Conference, Jiaxing has complex air pollution features in winter that can be impacted by local emissions and also emissions transported from the surrounding cities of Shanghai and Hangzhou. In addition, the prevailing air flow from the northwest can convey pollutants from the North China Plain to the YRD region. However, the research pertaining to the air quality during the WIC has not been studied to present. Hence, this study can provide some references for the air quality control strategy of subsequent WICs. Moreover, the information obtained about the mixing state and the temporal variation of particle types is essential for developing an understanding of the origin and evolution processes of atmospheric aerosols in the YRD.

2 Instruments and experiments

2.1. Observation site and experiment description

Measurements were conducted on the 4th floor of the Jiaxing Environmental Monitoring Station (30.76° N, 120.77° E, 15 m a.s.l.). The site information is shown in Figure 1. Jiaxing is located in northeastern Zhejiang Province and is less than 100 km from Shanghai, Hangzhou, Ningbo, Shaoxing, and Suzhou. As a typical coastal city in the YRD region, Jiaxing is 32 km from Hangzhou Bay, 38 km from Taihu, and 20 km from Wuzhen, where the WIC was held (Figure 1). According to Figure 1, there are no obvious fire points around the observation site, indicating that no biomass burning processes occurred. These observations were carried out during December

11-25, 2015.

2.2. Instrumentation

Trace gases consisting of O_3, SO_2, NO_2, and CO were observed with a time resolution of 1 h using online analyzers (Thermo Instruments, TEI 49i, 43i, 42i, and 48i, respectively), and $PM_{2.5}$ and PM_{10} mass concentrations were observed with a resolution of 1 h using a mass analyzer (Thermo SHARP-5030). These instruments have been employed in many related studies (Ding et al., 2013; Hu et al., 2014). Ding et al. (2013) provides a more detailed introduction to the instrumentation.

The single particle aerosol mass spectrometer (SPAMS, Hexin Analytical Instrument Co., Ltd., China) used in this study was described in detail previously (Li et al., 2011; Wang et al., 2016). Air was sampled into the SPAMS inlet using a conductive silicone tube with an inner diameter of 6 mm and a length of ~2 m on the roof of a four-floor building. Aerosol particles were introduced into the SPAMS using an aerodynamic lens and then focused and accelerated to specific velocities determined by their flight times through two continuous diode Nd: YAG (neodymium: yttrium aluminum garnet) laser beams (532 nm) in the sizing region. The particle chemical composition was detected through the desorption/ionization process by using a 266 nm ultraviolet laser beam. Both the positive and negative ion fragments generated were recorded with vacuum aerodynamic diameter (d_{va}) (Zhang et al., 2013). Particle size and mass calibrations for this instrument were carried out every three months using standard polystyrene latex particles (PSL) and a metallic solution. Li et al. (2011) and Zhang et al. (2013, 2014, 2015) provide further details about the instrument.

The SPAMS data were analyzed using the YAADA software toolkit (http://www.yaada.org/) (Allen, 2008). All of the acquired mass spectra were imported into YAADA and further classified using the ART-2a adaptive resonance algorithm (Song et al., 1999). The parameters for the ART-2a analysis in this study included a vigilance factor of 0.75, a learning rate of 0.05, and a maximum of 20 iterations. Figure 2 shows that the single particle concentrations were positively correlated with $PM_{2.5}$ ($R = 0.6$). This result demonstrated that the SPAMS data could accurately represent the aerosol particle characteristics during the observation period.

2.3. Air mass backward trajectories

Air mass backward trajectories for 24 h of each day were simulated using the Hybrid

Single-Particle Lagrangian Integrated Trajectory (HYSPLIT, http://www.arl.noaa.gov/HYSPLIT_info.php) model developed by the National Oceanic and Atmospheric Administration (NOAA) Air Resources Laboratory (ARL). The backward trajectories were calculated at 12:00 (LST, local time) at a height of 1000 m above the observation sites (Figure 1). The National Weather Service National Centers for Environmental Prediction (NCEP) Global Data Assimilation System (GDAS) archive was used for meteorological input data. The GDAS data were obtained with a horizontal resolution of $1.0^{\circ} \times 1.0^{\circ}$.

2.4. The Multi-resolution Emission Inventory for China (MEIC) data

The Multi-resolution Emission Inventory for China (MEIC) (http://www.meicmodel.org/index.html) is a technology-based bottom-up air pollutant and greenhouse gas inventory of anthropogenic sources that is based on a cloud-computing platform and maintained by Tsinghua University. The $PM_{2.5}$ emission source data used in our study, including those from industry, traffic, power plants, and residences in December 2015, were provided by MEIC with a spatial resolution of $0.25^{\circ} \times 0.25^{\circ}$.

3. Results and discussion

3.1. Changes in PM and gas pollutant concentrations before, during, and after the WIC

The observation period was divided into three stages: before the WIC (from 15:00 on Dec. 11 to 00:00 on Dec. 16), during the WIC (from 00:00 on Dec. 16 to 16:00 on Dec. 18), and after the WIC (from 16:00 on Dec. 18 to 22:00 on Dec. 25). Figure 2 shows that the concentrations of PM and gas pollutants were high before the WIC but decreased significantly during the WIC due to the implemented reduction measures. Under the influences of boundary layer's diurnal variations, the air pollutants exhibited obvious diurnal variations with low concentrations at daytime and high concentrations at night in Dec., 2014 (Figure S1). Besides, the pollutant concentrations on Dec.16-18, 2014 were relatively low. The history weather map demonstrated that a strong cold air passed through Jiaxing, resulting in large wind speed. A gale yellow warning signal was published at 12:20 on Dec.16 by Jiaxing Meteorological Bureau and didn't relieve until 06:52 on Dec.17 (http://jx.zj.weather.com.cn). The minimum temperature reached to -6.5 ^{o}C on Dec.18. Therefore, meteorological conditions had great impacts on pollutant distributions. The phenomenon also occurred on Dec. 12, 19 and 24, 2015 (Figure 2). Table 1 lists the average concentrations of $PM_{2.5}$ and PM_{10}, which were 38.7 and 75.0 $\mu g \cdot m^{-3}$ during the WIC, made a reduction of 62.1 % , 47.1 %

and 43.8 % and 60.0 %, 45.7 % and 36.8 % compared to the levels before and after the WIC and Dec., 2014, respectively. Figure 1 shows that the air masses affecting the region from Dec. 16-18, 2015, arrived from the north. Although these trajectories passed by areas with high $PM_{2.5}$ pollution such as Shijiazhuang, Xuzhou, Jinan, Nanjing, and Changzhou on Dec. 16-17, the air mass trajectories were long and transmitted quickly, resulting in high wind speed. However, air masses originating above the Yellow Sea moved slowly and passed by areas with numerous $PM_{2.5}$ emission sources on Dec. 18, resulting in enhanced PM concentration in the morning.

Based on the weather map published by the Hong Kong Observatory (http://www.hko.gov.hk), Jiaxing was controlled by high-pressure periphery or high-pressure center on Dec. 11-15 and 19-25, resulting in scarce isobars and field pressure, which is unfavorable for pollutant dispersion. On Dec. 16-18, a cold air mass passed over the YRD region, leading to a temperature decrease of 4-6 °C and high winds (grades 4-5 based on the Beaufort scale), which favored the diffusion of pollutants. Therefore, the PM concentrations decreased during the WIC due to the favorable synoptic weather and the strict pollutant emission reduction.

Figure 2 shows complex variations of gaseous pollutants throughout the sampling period. The average concentrations of NO_2 and CO during the WIC were 43.5 $\mu g \cdot m^{-3}$ and 0.7 $mg \cdot m^{-3}$, representing decreases of 31.2 %, 41.7 % and 41.2 % and 34.7 %, 41.7 % and 22.2 % compared to the concentrations before and after the WIC in Dec., 2014, respectively. The sources of NO_2 and CO were mainly vehicle exhaust and industry emissions, and the atmospheric concentration decreases during the WIC were a result of the pollutant emission reduction measures. The SO_2 concentrations were relatively low at the beginning of the WIC, and the maximum value of 112 $\mu g \cdot m^{-3}$ occurred at 09:00 on Dec. 18. According to Figures 1 and 3, the air masses passed through areas with many industries and power plants, which emitted generous amounts of SO_2 gas, and further transported the emissions to Jiaxing. The O_3 concentration exhibited diurnal variations and was relatively high, with an average concentration of 31.2 $\mu g \cdot m^{-3}$ (Table 1) during the WIC, which is 1.1 and 1.6 times larger than the concentrations before and after the WIC, respectively. During the WIC, the sunny days were dominated and the solar radiation was strong, with the result of high O_3 concentrations. After the WIC, the cloudy or light rainy days were dominated and the solar radiation was weak, besides, the air masses, which arrived from southwest or eastern ocean areas, were clean, the O_3 concentrations were comparatively low. Table 1 reveals that the SO_2

concentrations during the WIC decreased by 22.5 % compared to the levels in December 2014, on the contrary, the O_3 concentrations during the WIC were 1.3 times larger than the levels in Dec., 2014. In conclusion, the emission control had relatively weak impacts on secondary pollutant.

3.2. Mixing state of aerosol particles

The prime peaks in the positive ion mass spectrum were 18$[NH_4]^+$, 23$[Na]^+$, 27$[Al]^+$, 39$[K]^+$, and EC cluster ions (12$[C]^+$, 24$[C_2]^+$, 36$[C_3]^+$,…, $[C_n]^+$) (Figure 4a). Other organic fragment signals were observed at 37$[C_3H]^+$, 43$[C_2H_5O]^+$, 50$[C_4H_2]^+$, 51$[C_4H_3]^+$, 61$[C_5H]^+$, 63$[C_5H_3]^+$, 77$[C_6H_6]^+$, 85$[C_7H]^+$, and 115$[C_9H_7]^+$. Moreover, there were many heavy metal signals in the positive mass spectra, such as m/z 51$[V]^+$, 55$[Mn]^+$, 56$[Fe]^+$, 63$[Cu]^+$, and 206-208$[Pb]^+$, and strong signals for secondary ions in the negative spectra, such as -46$[NO_2]^-$, -62$[NO_3]^-$, and -97$[HSO_4]^-$ (Figure 4b). Numerous EC cluster ions, such as (12$[C]^-$, 24$[C_2]^-$, 36$[C_3]^-$…, $[C_n]^-$), and -26$[CN]^-$, -35$[Cl]^-$, and -42$[CNO]^-$ were also observed. In addition, peaks corresponding to 30$[Si]^+$ and 7$[Li]^+$ in the positive mass spectra and -16$[O]^-$, -17$[OH]^-$, and -88$[FeO_2]^-$ in the negative mass spectra were observed. These compound particles may be attributed to distinct sources and/or extensive processing of aerosol particles (Zhang et al., 2013).

The chemical patterns of the aerosol were used to classify particles into distinct catalogues, which are listed in Table 2. The average positive and negative mass spectra of the main particle classes are shown in Figure 5. The particle clusters were categorized as (1) K-rich particles comprised of K-CN, K-Secondary, and K-mixed elemental carbon (K-EC) classes, (2) Sodium particles, (3) Carbonaceous particles, including EC-Nitrate, EC-Secondary, and OCEC (organics and elemental carbon) classes, (4) Ammonium particles, and (5) Heavy-metal particles, consisting of Fe-Secondary, Cu-V, and Pb particles. The mass spectral signatures of these clusters are described briefly below.

3.2.1. K-rich particles

The K-rich particles, which included K-CN, K-Secondary, and K-EC types, constituted 38.4% of the total particles. Figure 5 shows that the K-rich particles were characterized by strong K^+ signals and elevated signals at -46$[NO_2]^-$, -62$[NO_3]^-$, and -97$[HSO_4]^-$. K is usually considered to be a notable marker of biomass burning/biofuel sources (Bi et al., 2011). However, Hleis et al. (2013) demonstrated that K may also originate from steelwork sinter plants.

The K-CN particles were characterized by strong signals for 23$[Na]^+$, -26$[CN]^-$ and

-42[CNO]$^-$. Additionally, strong signals of levoglucosan ion fragments (-45[CHO_2]$^-$, -59[$C_2H_3O_2$]$^-$, -71[C_3H_3O]$^-$), which are considered to be unique markers of biomass burning (Silva et al., 1999), were detected. Hence, the K-CN particles, accounting for 5.8 % of the total particles, could originate from direct biomass/biofuel emissions, as shown in Table 2.

K-Secondary particles and K-EC particles constituted 19.9 % and 12.7 % of the total particles, respectively (Table 2). The signals of secondary ions of -46[NO_2]$^-$, -62[NO_3]$^-$, and -97[HSO_4]$^-$ in the two classes were much stronger than the signals for the K-CN particles, and the signals for 23[Na]$^+$ in the two classes were much weaker than the signals for the K-CN particles. The signals for -26[CN]$^-$ were weak, and levoglucosan ion fragments were scarcely observed in the two classes. Pratt et al. (2011) showed that levoglucosan can decay or even disappear due to oxidizing reactions in the atmosphere, which means that the K-Secondary particles and the K-EC particles had stronger aging processes. The K-EC particles were characterized by many EC cluster ions (12[C]$^{+/-}$, 24[C_2]$^{+/-}$, 36[C_3]$^{+/-}$,…, [C_n]$^{+/-}$) and 40[Ca]$^+$. The intense K signal may imply the origin of biomass/biofuel for the EC particles (Zhang et al., 2013). Potassium chloride (KCl) occurs in young smoke from biomass burning, whereas K_2SO_4 and KNO_3 concentrations increase as smoke ages due to the quick replacement of chloride by sulfate and nitrate during the transport process (Zauscher et al., 2013; Zhang et al., 2015). Calcium-containing EC particles from combusted lubricating oil have been explored previously in automobile exhaust (Dall'Osto et al., 2009). Therefore, the K-EC particles may originate from biomass, biofuels, and vehicle exhaust. Zhang et al. (2013) and Pratt et al. (2011) observed that biomass and biofuel particles were subjected to atmospheric aging and obtained sulfate and nitrate during transportation processes. Apart from the direct burning process, the K-Secondary particles originated more from aging processes of fresh particles.

3.2.2. Sodium particles

Sodium particles showed spectral signals at 23[Na]$^+$ and 39[K]$^+$ in the positive spectrum and at -46[NO_2]$^-$, -62[NO_3]$^-$, and -97[HSO_4]$^-$ in the negative spectrum and accounted for 11.8 % of the total particles. Figure 1 shows that the observation site is 32 km from Hangzhou Bay, which resulted in abundant sea-salt particles in the air. Consequently, various amounts of secondary inorganic particles could have formed by adsorption and the heterogeneous reaction processes attributed to these hygroscopic sea-salt particles. The existence of nitrate in the sodium particles

hinted the substitution of chloride by nitrate during long-distance transport (Gard et al., 1998). Additionally, weak signals from EC cluster ions and -26$[CN]^-$ suggested that the sea-salt particles may have adsorbed onto other aerosol particles through coagulation. However, Moffet et al. (2008b) suggested that this class may be from dust and industry sources.

3.2.3. Carbon-rich particles

Carbon-rich particles accounted for 34.2 % of the total particles, as shown in Table 2, and were composed of the following particle classes: EC-Nitrate, EC-Secondary, and OCEC. The EC-Nitrate and EC-Secondary particles were characterized by EC cluster ions (12$[C]^-$, 24$[C_2]^-$, 36$[C_3]^-$,…, $[C_n]^-$). The EC-Nitrate particle class showed strong peaks for -46$[NO_2]^-$ and -62$[NO_3]^-$ and had scarce signals for -97$[HSO_4]^-$. However, strong signals for -46$[NO_2]^-$, -62$[NO_3]^-$, and -97$[HSO_4]^-$ were observed in EC-Secondary particles. Moreover, the signals for EC cluster ions in EC-nitrate particles were much stronger than those in EC-secondary particles. This finding implied that EC particles that were absorbed by -97$[HSO_4]^-$ were transformed intensively and represented aged particles with low volatility; the opposite was true for EC particles absorbed by nitrate, which represented semi-volatile fresh particles. EC-Nitrate and EC-Secondary particles accounted for 3.8 % and 14.1 % of the total particles, respectively. The OCEC particles had typical EC cluster ions, with OC markers (e.g., 27$[C_2H_3]^+$, 39$[C_3H_3]^+$, 41$[C_3H_5]^+$, 50$[C_4H_2]^+$, 64$[C_5H_4]^+$, 75$[C_6H_3]^+$).

3.2.4. Ammonium particles

The ammonium particles showed spectral signals from 18$[NH_4]^+$, 39$[K]^+$, -46$[NO_2]^-$, -62$[NO_3]^-$, and -97$[HSO_4]^-$ and constituted 1.3 % of the total particles. The ammonium in air is from a variety of sources, including sewage treatment, animal husbandry, waste incineration, the marine environment, biomass burning, industrial processes, and vehicle exhaust (Cadle et al., 1980; Moffet et al., 2008b). Moreover, gaseous precursors (nitric acid and ammonia) may be converted into secondary aerosols, e.g., ammonium nitrate, during hazy days (Seinfeld and Pandis, 2012; Yang et al., 2012).

3.2.5. Heavy metal particles

Heavy metal particles, consisting of Fe-Secondary, Cu-V, and Pb particles, constituted 14.3 % of the total particles. Fe-Secondary particles constituted 6.7 % of the total particles and exhibited strong signals at m/z 56$[Fe]^+$, 39$[K]^+$, -46$[NO_2]^-$, and -62$[NO_3]^-$ and weak signals at m/z -97$[HSO_4]$

and 23$[Na]^+$. Fe-Secondary particles may be emitted through iron/steel industrial activities, coal combustion, and biomass burning (Chen et al., 2012; Zhang et al., 2014). Zhang et al. (2014, 2015) found that nitrate was a primary component in all the Fe-containing particle types and that sulfate and ammonium were present among K-rich particles in Shanghai and Guangzhou. The Cu-V particle class accounted for 6.4 % of the total particles and had positive spectra with strong signals at m/z 27$[Al]^+$, 43$[AlO]^+$, 39$[K]^+$, 51$[V]^+$, and 63$[Cu]^+$ and negative spectra with strong signals at -26$[CN]^-$, -46$[NO_2]^-$, -62$[NO_3]^-$, and -97$[HSO_4]^-$. The minor fraction of vanadium is attributed majorly to emissions from ship transportation and vehicle exhaust (Ault et al., 2010; Sodeman et al., 2005). Al/AlO-Nitrate particles normally originate from traffic and from the secondary transformation process (Taiwo et al., 2014). Cu is generally emitted from industries, foundries, and traffic (Fernández et al., 2000). Lead particles constituted 1.2 % of the total particles and showed strong peaks for 39$[K]^+$, 208$[Pb]^+$, -46$[NO_2]^-$, and -62$[NO_3]^-$ and weak peaks for 23$[Na]^+$ and -35$[Cl]^-$. The major emission sources of Pb include automobile exhaust, oil combustion, aviation gasoline combustion (piston engine), the metallurgy and cement industries, and coal combustion (Moffet et al., 2008; Wang et al., 2000). Moffet et al. (2008a) suggested that heavy metal particles containing chloride and nitrate salts had been observed in the urban atmosphere and attributed these particle types to industrial waste incineration.

3.3. Temporal characteristics and size distributions of particles

Figure 6 illustrates that aerosol concentrations decreased significantly during the WIC and increased sharply after WIC. The concentrations increased by 52.0 % within 1 hour at 22:00 on Dec. 18 but decreased rapidly 4 hours later. The explosive growth of particles from 20:00 on Dec. 18-01:00 on Dec. 19 were mainly induced by the sharp increase of OCEC particles sized 0.4-0.8 μm according to figure 6 and figure S2. Previous study demonstrated that OCEC particles were mainly from industrial emissions and quite possibly related to incineration or refuse burning and vehicle exhausts (Moffet et al., 2008b; Wang et al., 2015; Zhang et al., 2013). The air masses corresponding to that episode mainly passed through Shanghai and Suzhou with high industrial and vehicle emissions (Figure S3 and figure 3). After the WIC, the industrial and vehicle emissions increased as the emission control canceled. Additionally, the boundary layer lowered at night. As a result, the pollutants grown sharply especially for the OCEC particles emitted by industry and vehicle exhaust. The minimum aerosol level was reached at 13:30 on Dec. 19 and the level then

increased slowly.

The chemical components of aerosol particles changed over the observation time, as shown in Figure 6. The K-CN and OCEC particles increased during the WIC, accounting for 15.3 % and 27.5 % of the total particles, compared with 4.9 % and 15.2 % before and 3.8 % and 14.0 % after the WIC, respectively (Figure 7). Figure 3 shows that many power plants and traffic sources are distributed throughout the area surrounding Jiaxing (including Hangzhou, Shanghai, Changzhou, and Suzhou), where air masses passed during the WIC (Figure 1). Therefore, the concentrations of K-CN and OCEC particles were high due to these direct emissions. The analyses described above indicated that weather conditions were stable before and after the WIC, so the aerosol particles were consequently prone to aging, leading to low proportions of K-CN and OCEC particles. The Cu-V particles constituted 16.8 % of the total particles during the WIC and constituted 4.6 % before and 4.5 % after the WIC, respectively, as shown in Figure 6. The previous analyses showed that the Cu-V particles originated from industry and automobile traffic. Figure 3 also reveals that large numbers of industrial sites are located around Jiaxing. Hence, the Cu-V particles may have originated in the surrounding cities. Before and after the WIC, westerly and southerly air masses were dominant (Figure 1), respectively, with few trajectories passing through Shanghai, Suzhou, and Changzhou; consequently, the Cu-V particle concentrations were low.

During the WIC, the concentrations of K-EC, EC-Secondary, and Fe-Secondary particles clearly decreased (Figure 6), constituting 4.5 %, 2.0 %, and 1.9 % of the total particles, respectively. These particles accounted for 12.5 %, 15.0 %, and 5.2 % and 14.7 %, 16.7 %, and 8.3 % of the total particles before and after the WIC, respectively (Figure 7). Figure 6b demonstrates that the average K-Secondary particle concentration during the WIC was 343 h^{-1}, which was lower by 17.0 % and 43.0 % compared to the levels before and after the WIC, respectively. However, the proportion of K-Secondary particles to total particles during the WIC was 17.2 %, which was lower by only 5.0 % and 2.6 % compared to before and after the WIC, respectively, due to the low background concentration of total particles. In addition, the Pb particle concentration varied slightly during the observation period (Figure 6) and had small proportions of 1.4 %, 2.0 %, and 1.0 % before, during, and after the WIC (Figure 7), respectively, which illustrates that the industry emissions surrounding Jiaxing have large impacts on air quality.

Figure 6 shows that the sodium particles changed slightly over the observation period and

occupied 13.6 %, 11.6 %, and 11.2 % of the total particles before, during, and after the WIC, respectively. The proportions of EC-Nitrate and ammonium particles were low, with values of 0.5 % and 0.7 %, respectively, during the WIC. Aerosol particles from primary emissions and transmission from surrounding areas were dominant, and the weather conditions were favorable for pollution diffusion; therefore, the primary and secondary pollutants were low during the WIC.

Figure 8 shows that the aerosol size spectra had unimodal distributions during the observation period. During the WIC, the peaks of different particle types shifted to fine particle segments (0.5-0.6 μm) and the peak width became relatively narrow. In the rest of the sampling period, broader peaks represented particles sized 0.5-0.7 μm before the WIC and 0.6-0.8 μm after the WIC. However, the size distributions of K-CN particles were identical throughout the sampling period, as shown in Figure 8, with peaks at 0.5-0.6 μm, indicating that this particle type had a weak aging process.

Figure 8 reveals that the chemical components of aerosols sized 0.2-0.4 μm, which were dominated by K-CN and sodium particles, were similar in the three sampling periods. The proportion of K-CN particles sized 0.4-0.6 μm decreased from 26.0 % during the WIC to 4.0 % before and after WIC. Among the aerosols sized 0.4-1.4 μm during the WIC, the K-CN particles had a high ratio and decreased slowly with size. The OCEC particles and Cu-V particles had large proportions of particles sized 0.4-1.4 μm, and the EC-Secondary, Fe-Secondary, and K-EC particles had small proportions. As a result, the air pollution control had a large impact on aerosol compositions sized 0.4-1.4 μm. The spectra distributions of sodium particles sized 0.4-1.4 μm were similar throughout the observation period and affected little by the air pollution control due to their origin from sea salt. Aerosols sized 1.4-2.0 μm were dominated by K-Secondary and sodium particles.

4. Conclusions

As the permanent venue for the World Internet Conference, Jiaxing implemented strict pollution-control measures during the 2nd WIC. In this study, particulate matter ($PM_{2.5}$ and PM_{10}), trace gases (CO, NO_2, SO_2, and O_3), and size-resolved mixing state of aerosol particles with 0.2-2.0 μm size were measured from December 11-25, 2015. We analyzed the impacts of emission controls on air pollutants during the WIC. In addition, the influences of air masses and emission sources on air pollutants were evaluated by using the HYSPLIT model and MEIC data.

During the WIC, the average concentrations of $PM_{2.5}$, PM_{10}, NO_2, and CO in Jiaxing were 38.7, 75.0, and 43.5 $\mu g \cdot m^{-3}$ and 0.7 $mg \cdot m^{-3}$, respectively, and these were decreased by 62.1 %, 47.1 %, 31.2 %, and 41.7 % and by 60.0 %, 45.7 %, 34.7 %, and 41.7 % compared to the levels before and after the WIC, respectively, which indicated that the emission controls on vehicles and industry sources had significant effects. The SO_2 concentrations during the WIC were high, with an average of 43.3 $\mu g \cdot m^{-3}$, due to the impacts of foreign transport. The average O_3 concentration during the WIC was 31.2 $\mu g \cdot m^{-3}$, which was 1.1 and 1.6 times larger than the values before and after WIC, respectively. The increased O_3 was due mainly to strong photochemical reaction under low PM concentrations.

This paper also provided detailed size, mass spectral, and temporal characteristics of the individual particles in the atmosphere of Jiaxing. In total, 877,397 particles were ionized, and 11 clusters were recognized with the assistance of YAADA 2.1. These clusters were sorted into five particle groups: K-rich (38.4 %), sodium (11.8 %), carbon-rich (34.2 %), ammonium (1.3 %), and heavy metal (14.3 %), which occupied 96.0 % of the successfully ionized particles. Signals of $23[Na]^+$ at different intensities were observed in the 11 clusters of particles, which may have been affected by sea salt particles in the coastal city of Jiaxing.

During the WIC, the proportions of K-EC (4.5 %), EC-Secondary (2.0 %), Fe-Secondary (1.9 %), EC-Nitrate (0.5 %), and ammonium (0.7 %) particles decreased significantly; those of K-CN (15.2 %), OCEC (27.5 %), and Cu-V (16.8 %) increased; and those of K-Secondary (17.2 %), sodium (11.6 %), and Pb (2.0 %) varied only slightly. The aerosol size spectra under different types of particles had unimodal distributions during the observation period. During the WIC, the peaks of different particle types shifted to fine particle segments (0.5-0.6 μm) and the peak width was relatively narrowed. In the rest of the sampling period, broadened peaks were observed for 0.5-0.7 μm sized particles before and 0.6-0.8 μm sized particles after the WIC. The air pollution control had large impacts on the K-CN, OCEC, Cu-V, EC-Secondary, Fe-Secondary, and K-EC particles sized 0.4-1.4 μm. The analysis revealed the physical and chemical properties of various particle types and their influence factors in the atmosphere of Jiaxing, which should be considered in predictions of their impacts on the environment.

Acknowledgments

This work was supported by grants from the national key research and development (R&D)

plan of China (2016YFA0602003), National Natural Science Foundation of China (91544229 and 41275143), the Open Fund by Jiangsu Key Laboratory of Atmospheric Environment Monitoring and Pollution Control (KHK1408) and the Research of $PM_{2.5}$ Source Apportionment and Control Technology in Jiaxing (2014AY21012).

References

Allen, J.O., 2008. YAADA: Software Toolkit to Analyze Single-particle Mass Spectral Data.

Ault, A.P., Gaston, C.J., Wang, Y., Dominguez, G., Thiemens, M.H., Prather, K.A., 2010. Characterization of the single particle mixing state of individual ship plume events measured at the port of Los Angeles. Environ. Sci. Technol. 44(6), 1954-1961

Bi, X., Zhang, G., Li, L., Wang, X., Li, M., Sheng, G., Fu, J., Zhou, Z., 2011. Mixing state of biomass burning particles by single particle aerosol mass spectrometer in the urban area of PRD, China. Atmos. Environ. 45(20), 3447-3453.

Cadle, S.H., Mulawa, P.A., 1980. Low-molecular-weight aliphatic amines in exhaust from catalyst-equipped cars. Environ. Sci. Technol. 14(6), 718-723.

Cao, J., Wang, Q., Chow, J.C., Watson, J.G., Tie, X., Shen, Z., Wang, P., An, Z., 2012. Impacts of aerosol compositions on visibility impairment in Xi'an, China. Atmos. Environ. 59: 559-566.

Chen, H., Laskin, A., Baltrusaitis, J., Gorski, C.A., Scherer, M. M., Grassian, V.H., 2012. Coal fly ash as a source of iron in atmospheric dust. Environ. Sci. Technol. 46(4), 2112-2120.

Cheng, Z., Wang, S., Jiang, J., Fu, Q., Chen, C., Xu, B., Yu, J., Fu, X., Hao, J., 2013. Long-term trend of haze pollution and impact of particulate matter in the Yangtze River Delta, China. Environ. Pollut. 182: 101-110.

Dall'Osto, M., Harrison, R.M., Coe, H., Williams, P., 2009. Real-time secondary aerosol formation during a fog event in London. Atmos. Chem. Phys. 9(7), 2459-2469.

Demayo, A., Taylor, M.C., Taylor, K.W., Hodson, P.V., Hammond, P.B., 1982. Toxic effects of lead and lead compounds on human health, aquatic life, wildlife plants, and livestock. Crit. Rev. Env. Sci. Tec. 12(4): 257-305.

Ding, A.J., Fu, C.B., Yang, X.Q., Sun, J.N., Zheng, L.F., Xie, Y.N., Herrmann, E., Petäjä, T., Kerminen, V.M., Kulmala, M., 2013a. Ozone and fine particle in the western Yangtze River Delta: an overview of 1 yr data at the SORPES station. Atmos. Chem. Phys. 13(11), 5813-5830.

480 Fernández, A.J., Ternero, M., Barragán, F.J., Jiménez, J.C., 2000. An approach to characterization
481 of sources of urban airborne particles through heavy metal speciation. Chemosphere, 2(2),
482 123-136.
483 Fu, Q., Zhuang, G., Wang, J., Xu, C., Huang, K., Li, J., Hou, B., Lu, T., Streets, D.G., 2008.
484 Mechanism of formation of the heaviest pollution episode ever recorded in the Yangtze River
485 Delta, China. Atmos. Environ. 42(9): 2023-2036.
486 Fuller, K.A., Malm, W.C., Kreidenweis, S.M., 1999. Effects of mixing on extinction by
487 carbonaceous particles. J. Geophys. Res. 104(15): 941-954.
488 Gard, E.E., Kleeman, M.J., Gross, D.S., Hughes, L.S., Allen, J.O., Morrical, B.D., Fergenson, D.P.,
489 Dienes, T., Galli, M.E., Johnson, R.J., Cass, G.R., Cass, G.R., 1998. Direct observation of
490 heterogeneous chemistry in the atmosphere. Science 279(5354), 1184-1187.
491 Haywood, J.M., Ramaswamy, V., Soden, B.J., 1999. Tropospheric aerosol climate forcing in
492 clear-sky satellite observations over the oceans. Science 283(5406): 1299-1303.
493 Healy, R.M., Sciare, J., Poulain, L., Crippa, M., Wiedensohler, A., Prévôt, A.S.H., Baltensperger,
494 U., Sarda-Estève, R., McGuire, M.L., Jeong, C.H., McGillicuddy, E., O'Connor, I.P., Sodeau,
495 J.R., Evans, G.J., Wenger, J.C., 2013. Quantitative determination of carbonaceous particle
496 mixing state in Paris using single-particle mass spectrometer and aerosol mass spectrometer
497 measurements. Atmos. Chem. Phys. 13(18): 9479-9496.
498 Hildemann, L.M., Markowski, G.R., Cass, G.R., 1991. Chemical composition of emissions from
499 urban sources of fine organic aerosol. Environ. Sci. Technol. 25(4): 744-759.
500 Hleis, D., Fernández-Olmo, I., Ledoux, F., Kfoury, A., Courcot, L., Desmonts, T., Courcot, D.,
501 2013. Chemical profile identification of fugitive and confined particle emissions from an
502 integrated iron and steel making plant. J. Hazard. Mater., 250, 246-255.
503 Hu, J., Wang, Y., Ying, Q., Zhang, H., 2014. Spatial and temporal variability of $PM_{2.5}$ and PM_{10}
504 over the North China Plain and the Yangtze River Delta, China. Atmos. Environ. 95:
505 598-609.
506 Kang, H., Zhu, B., Su, J., Wang, H., Zhang, Q., Wang, F., 2013. Analysis of a long-lasting haze
507 episode in Nanjing, China. Atmos. Res., 120, 78-87.
508 Kim, K.H., Jahan, S.A., Kabir, E., Brown, R.J., 2013. A review of airborne polycyclic aromatic
509 hydrocarbons (PAHs) and their human health effects. Environ. Int. 60: 71-80.

Kulmala, M., Vehkamäki, H., Petäjä, T., Dal Maso, M., Lauri, A., Kerminen, V.M., Birmili, W., McMurry, P.H., 2004. Formation and growth rates of ultrafine atmospheric particles: a review of observations. J. Aerosol Sci. 35(2): 143-176.

Li, L., Huang, Z., Dong, J., Li, M., Gao, W., Nian, H., Fu, Z., Zhang, G., Bi, X., Cheng, P., Zhou, Z., 2011. Real time bipolar time-of-flight mass spectrometer for analyzing single aerosol particles. Int. J. Mass Spectrom., 303 (2), 118-124.

Li, W., Shao, L., Zhang, D., Ro, C.U., Hu, M., Bi, X., Geng, H., Matsuki, A., Niu, H., Chen, J., 2016. A review of single aerosol particle studies in the atmosphere of East Asia: morphology, mixing state, source, and heterogeneous reactions. J. Clean. Prod. 112: 1330-1349.

Moffet, R.C., Desyaterik, Y., Hopkins, R.J., Tivanski, A.V., Gilles, M.K., Wang, Y., Shutthanandan, V., Molina, L.T., Abraham, R.G., Johnson, K.S., Mugica, V., Molina, Mario J.; Laskin, A., Mugica, V., 2008a. Characterization of aerosols containing Zn, Pb, and Cl from an industrial region of Mexico City. Environ. Sci. Technol. 42(19), 7091-7097.

Moffet, R.C., Foy, B.D., Molina, L.A., Molina, M.J., Prather, K.A., 2008b. Measurement of ambient aerosols in northern Mexico City by single particle mass spectrometry. Atmos. Chem. Phys. 8(16), 4499-4516.

Murphy, D.M., Cziczo, D.J., Froyd, K.D., Hudson, P.K., Matthew, B.M., Middlebrook, A.M., Peltier, R.E., Sullivan, A., Thomson, D.S., Weber, R.J., 2006. Single-particle mass spectrometry of tropospheric aerosol particles. J. Geophys. Res. 111(D23): DOI: 10.1029/2006JD007340.

Pósfai, M., Buseck, P.R., 2010. Nature and climate effects of individual tropospheric aerosol particles. Annu. Rev. Earth Planet. Sci. 38, 17-43.

Pratt, K.A., Murphy, S.M., Subramanian, R., DeMott, P.J., Kok, G.L., Campos, T., Rogers, D.C., Prenni, A.J., Heymsfield, A.J., Seinfeld, J.H., Prather, K.A., 2011. Flight-based chemical characterization of biomass burning aerosols within two prescribed burn smoke plumes. Atmos. Chem. Phys., 11(24), 12549-12565.

Seinfeld, J.H., Pandis, S.N., 2012. Atmospheric chemistry and physics: from air pollution to climate change. John Wiley & Sons.

Silva, P.J., Liu, D.Y., Noble, C.A., Prather, K.A., 1999. Size and chemical characterization of individual particles resulting from biomass burning of local Southern California species.

Environ. Sci. Technol. 33(18), 3068-3076.

Sodeman, D.A., Toner, S.M., Prather, K.A., 2005. Determination of single particle mass spectral signatures from light-duty vehicle emissions. Environ. Sci. Technol. 39(12), 4569-4580.

Song, X.H., Hopke, P.K., Fergenson, D.P., Prather, K.A., 1999. Classification of single particles analyzed by ATOFMS using an artificial neural network, ART-2A. Anal. Chem., 71(4): 860-865.

Sun, Y.L., Wang, Z.F., Fu, P.Q., Yang, T., Jiang, Q., Dong, H.B., Li, J., Jia, J.J., 2013. Aerosol composition, sources and processes during wintertime in Beijing, China. Atmos. Chem. Phys. 13(9): 4577-4592.

Sun, Y.L., Zhuang, G.S., Wang, Y., Han, L., Guo, J., Dan, M., Zhang, W., Wang, Z., Hao, Z., 2004. The air-borne particulate pollution in Beijing: concentration, composition, distribution and sources. Atmos. Environ. 38(35): 5991-6004.

Taiwo, A.M., Harrison, R.M., Beddows, D.C., Shi, Z., 2014. Source apportionment of single particles sampled at the industrially polluted town of Port Talbot, United Kingdom by ATOFMS. Atmos. Environ. 97, 155-165.

Vogt, R., Kirchner, U., Scheer, V., Hinz, K.P., Trimborn, A., Spengler, B., 2003. Identification of diesel exhaust particles at an Autobahn, urban and rural location using single-particle mass spectrometry. J. Aerosol Sci. 34(3): 319-337.

Wang, H., An, J., Shen, L., Zhu, B., Xia, L., Duan, Q., Zou, J., 2016. Mixing state of ambient aerosols in Nanjing city by single particle mass spectrometry. Atmos. Environ. 132: 123-132.

Wang, J., Guo, P., Li, X., Zhu, J., Reinert, T., Heitmann, J., Spemann, D., Vogt, J., Flagmeyer, R.H., Butz, T., 2000. Source identification of lead pollution in the atmosphere of Shanghai City by analyzing single aerosol particles (SAP). Environ. Sci. Technol. 34(10): 1900-1905

Yang, F., Chen, H., Du, J., Yang, X., Gao, S., Chen, J., Geng, F., 2012. Evolution of the mixing state of fine aerosols during haze events in Shanghai. Atmos. Res. 104, 193-201.

Zauscher, M.D., Wang, Y., Moore, M.J., Gaston, C.J., Prather, K.A., 2013. Air quality impact and physicochemical aging of biomass burning aerosols during the 2007 San Diego wildfires. Environ. Sci. Technol. 47(14), 7633-7643

Zhang, G., Bi, X., Li, L., Chan, L. Y., Li, M., Wang, X., Sheng, G., Fu, J., Zhou, Z., 2013. Mixing state of individual submicron carbon-containing particles during spring and fall seasons in

570 urban Guangzhou, China: a case study. Atmos. Chem. Phys., 13(9), 4723-4735.
571 Zhang, G., Bi, X., Lou, S., Li, L., Wang, H., Wang, X., Zhou, Z., Sheng, G., Fu, J., Chen, C., 2014.
572 Source and mixing state of iron-containing particles in Shanghai by individual particle
573 analysis. Chemosphere, 95, 9-16.
574 Zhang, G., Han, B., Bi, X., Dai, S., Huang, W., Chen, D., Wang, X., Sheng, G., Fu, J., Zhou, Z.,
575 2015. Characteristics of individual particles in the atmosphere of Guangzhou by single
576 particle mass spectrometry. Atmos. Res. 153, 286-295.
577 Zhang, R., 2010. Getting to the critical nucleus of aerosol formation. Science 328(5984):
578 1366-1367.
579 Zhu, T., Shang, J., Zhao, D.F., 2011. The roles of heterogeneous chemical processes in the
580 formation of an air pollution complex and gray haze. Sci. China Chem. 54(1): 145-153.
581 Li, S. W., Li, H. B., Luo, J., Li, H. M., Qian, X., Liu, M. M., ... & Ma, L. Q. (2016). Influence of
582 pollution control on lead inhalation bioaccessibility in PM 2.5: A case study of 2014 Youth
583 Olympic Games in Nanjing. Environment international, 94, 69-75
584 Wang, Y., Zhang, Y., Schauer, J. J., de Foy, B., Guo, B., & Zhang, Y. (2016). Relative impact of
585 emissions controls and meteorology on air pollution mitigation associated with the
586 Asia-Pacific Economic Cooperation (APEC) conference in Beijing, China. Science of The
587 Total Environment
588 Sun, Y., Wang, Z., Wild, O., Xu, W., Chen, C., Fu, P., ... & Wang, Q. (2016). “APEC Blue”:
589 Secondary Aerosol Reductions from Emission Controls in Beijing. Scientific reports, 6
590 Zhou, Y., Wu, Y., Yang, L., Fu, L., He, K., Wang, S., ... & Li, C. (2010). The impact of
591 transportation control measures on emission reductions during the 2008 Olympic Games in
592 Beijing, China. Atmospheric Environment, 44(3), 285-293
593 Wang, S., Zhao, M., Xing, J., Wu, Y., Zhou, Y., Lei, Y., ... & Hao, J. (2010). Quantifying the air
594 pollutants emission reduction during the 2008 Olympic Games in Beijing. Environmental
595 Science & Technology, 44(7), 2490-2496
596 Wang, T., Nie, W., Gao, J., Xue, L. K., Gao, X. M., Wang, X., ... & Wang, S. L. (2010). Air quality
597 during the 2008 Beijing Olympics: secondary pollutants and regional impact. Atmospheric
598 Chemistry and Physics, 10(16), 7603-7615
599 Wang, W., Primbs, T., Tao, S., & Simonich, S. L. M. (2009). Atmospheric particulate matter

pollution during the 2008 Beijing Olympics. Environmental Science & Technology, 43(14), 5314-5320

Tables and Figures

Supplementary Material

Table 1. Concentrations of particulate matter (PM) and trace gases

	$PM_{2.5}$(μg·m^{-3})	PM_{10}(μg·m^{-3})	SO_2(μg·m^{-3})	NO_2(μg·m^{-3})	CO(mg·m^{-3})	O_3(μg·m^{-3})
Before WIC	102.0	141.7	46.7	63.2	1.2	27.3
WIC	38.7	75.0	43.3	43.5	0.7	31.2
After WIC	96.8	138.1	30.9	66.6	1.2	19.5
Dec. 2014	68.9	118.6	55.9	74.0	0.9	24.3

Table 2. Summary of the number count and fraction of single-particle classes during the observation period

Particle classes	Single particle classes	Number count	Number fraction
K-rich		322383	38.4%
	K-CN	48935	5.8%
	K-secondary	167320	19.9%
	K-EC	106728	12.7%
Sodium	K-Na	98973	11.8%
Carbon-rich		287620	34.2%
	EC-nitrate	32335	3.8%
	EC-Secondary	118347	14.1%
	OCEC	136938	16.3%
Ammonium	Ammonium	10907	1.3%
Heavy-Metal		120166	14.3%
	Fe-Secondary	55874	6.7%
	Cu-V	54143	6.4%
	Pb	10149	1.2%

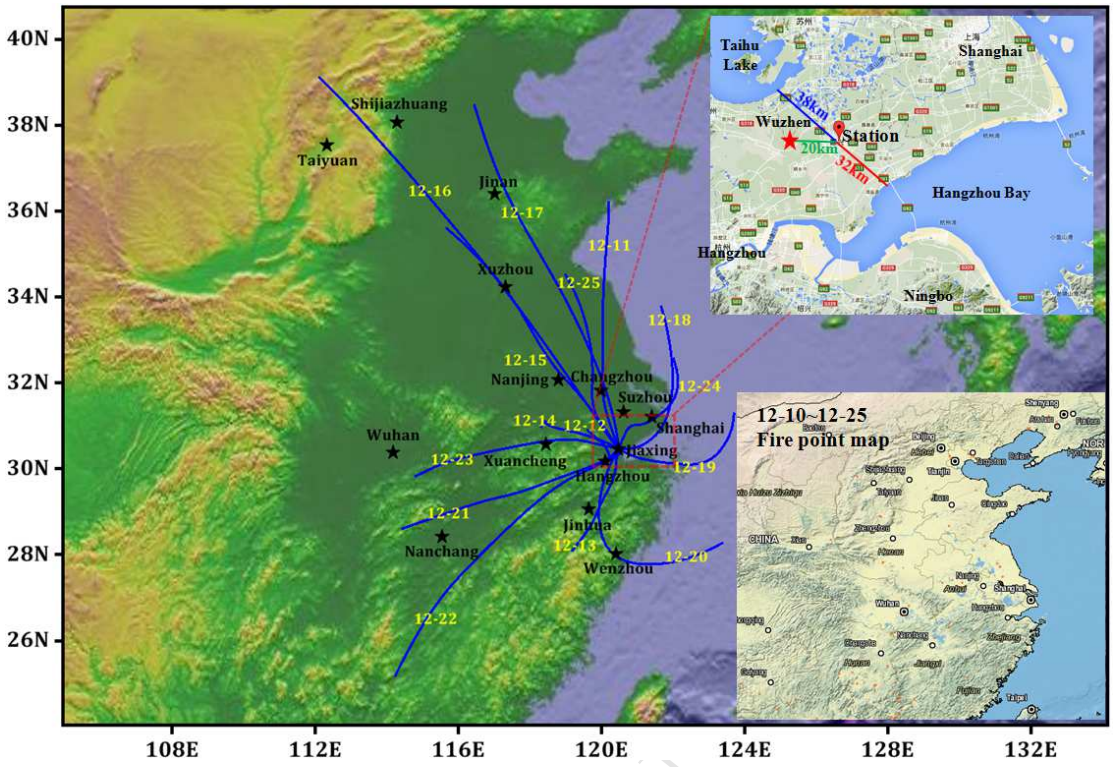

Figure 1 Site information, fire point map and the daily backward trajectories at 12:00 LST and 1000 m a.s.l. during the observation periods

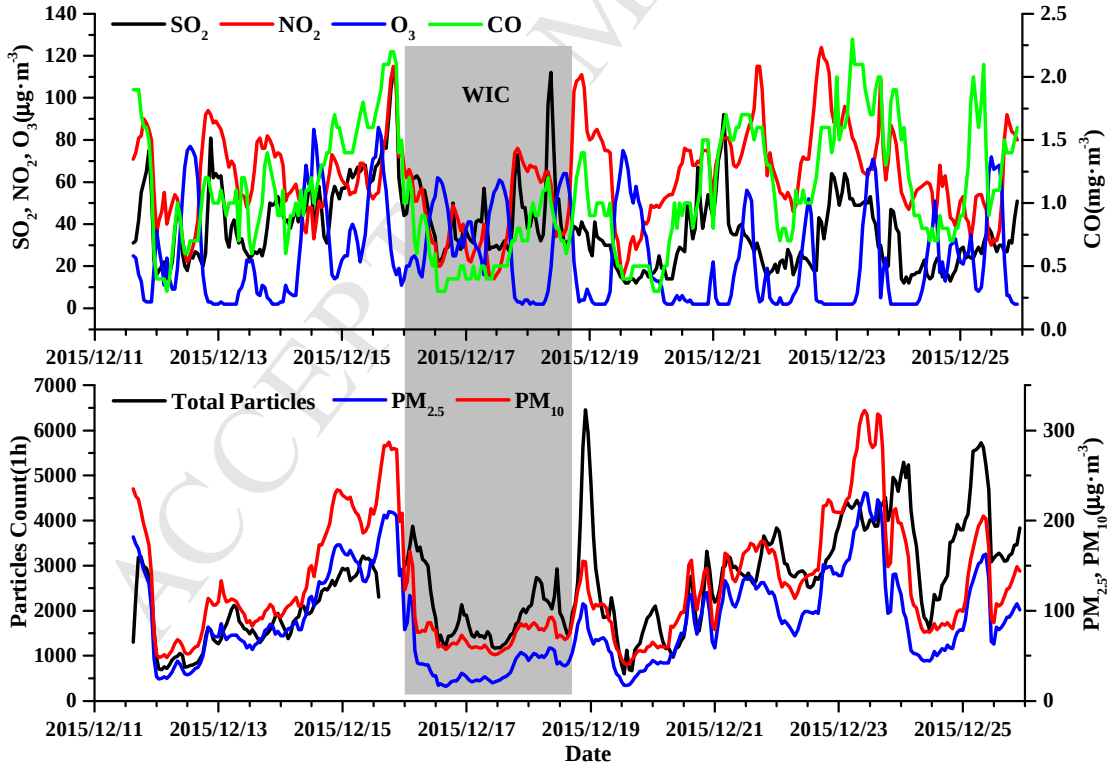

Figure 2. Time series of particulate matter (PM) and trace gas concentrations

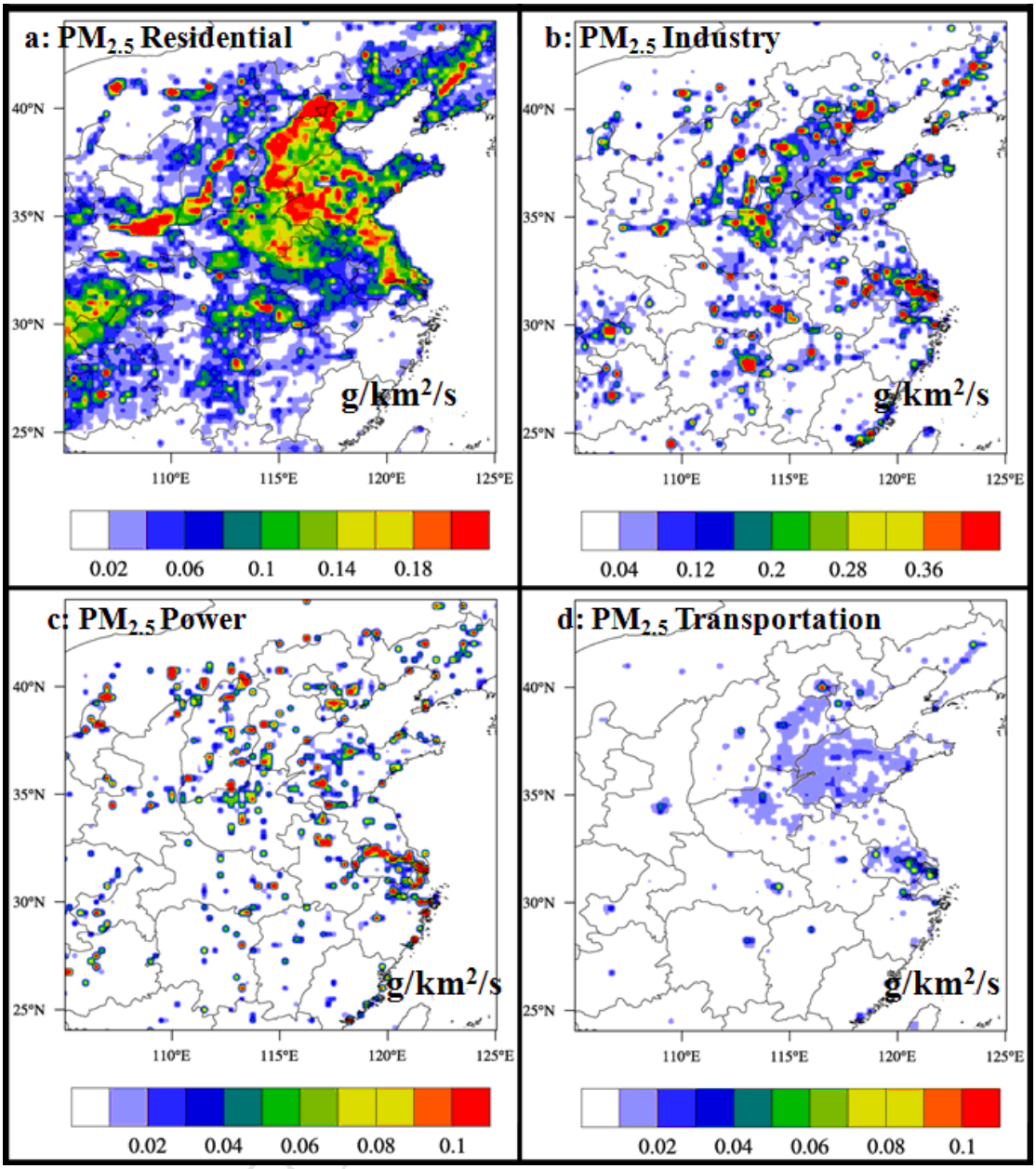

Figure 3 Plots of $PM_{2.5}$ emission sources from the Multi-resolution Emission Inventory for China (MEIC) in December

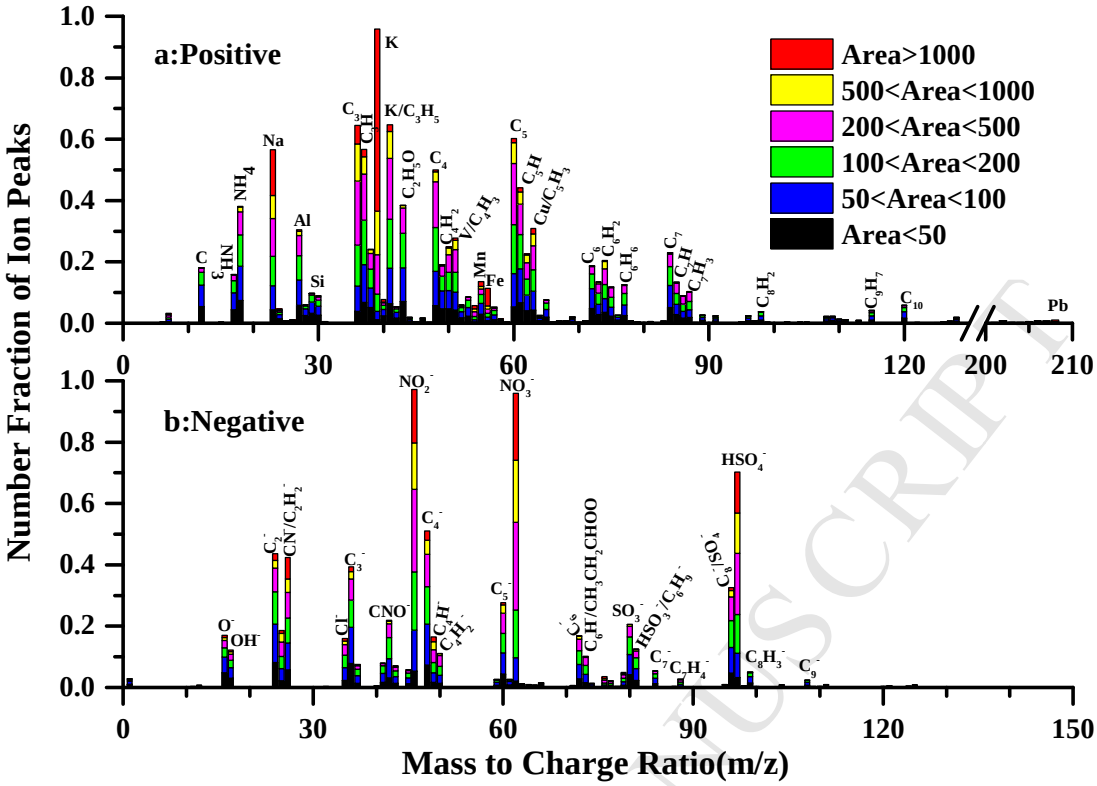

Figure 4. Average digitized positive (a) and negative (b) ion mass spectrum of aerosol particles during the observed period

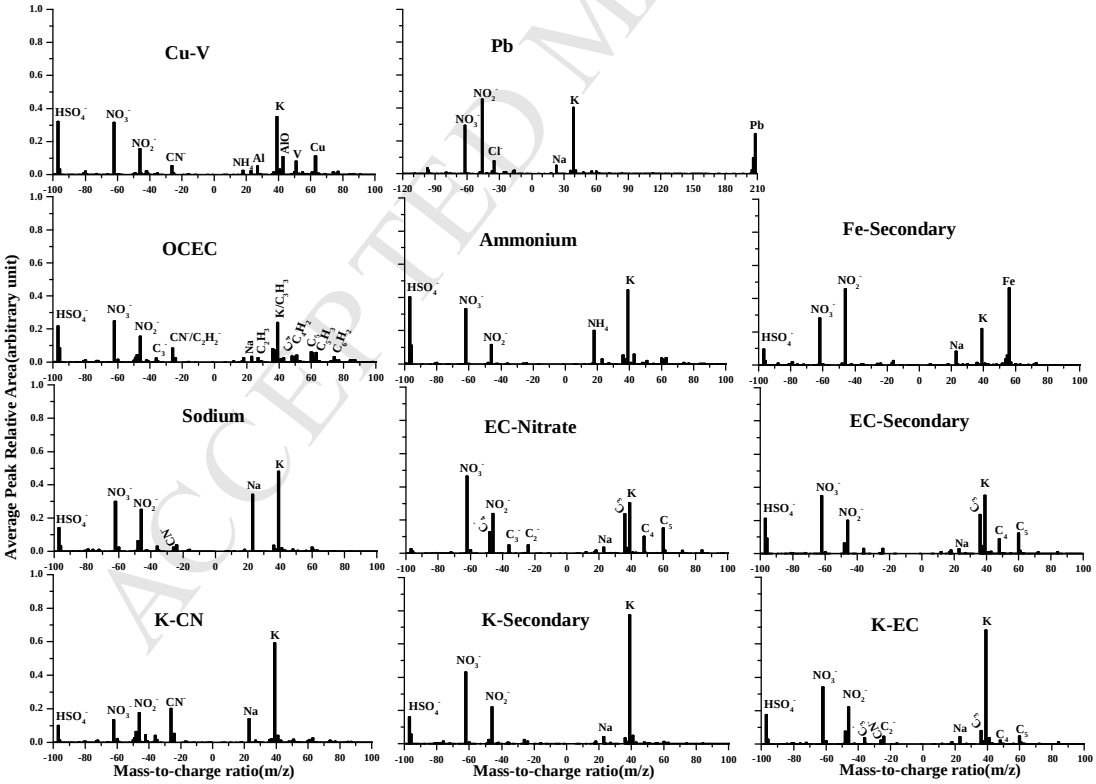

Figure 5. Average positive and negative mass spectra for each particle class

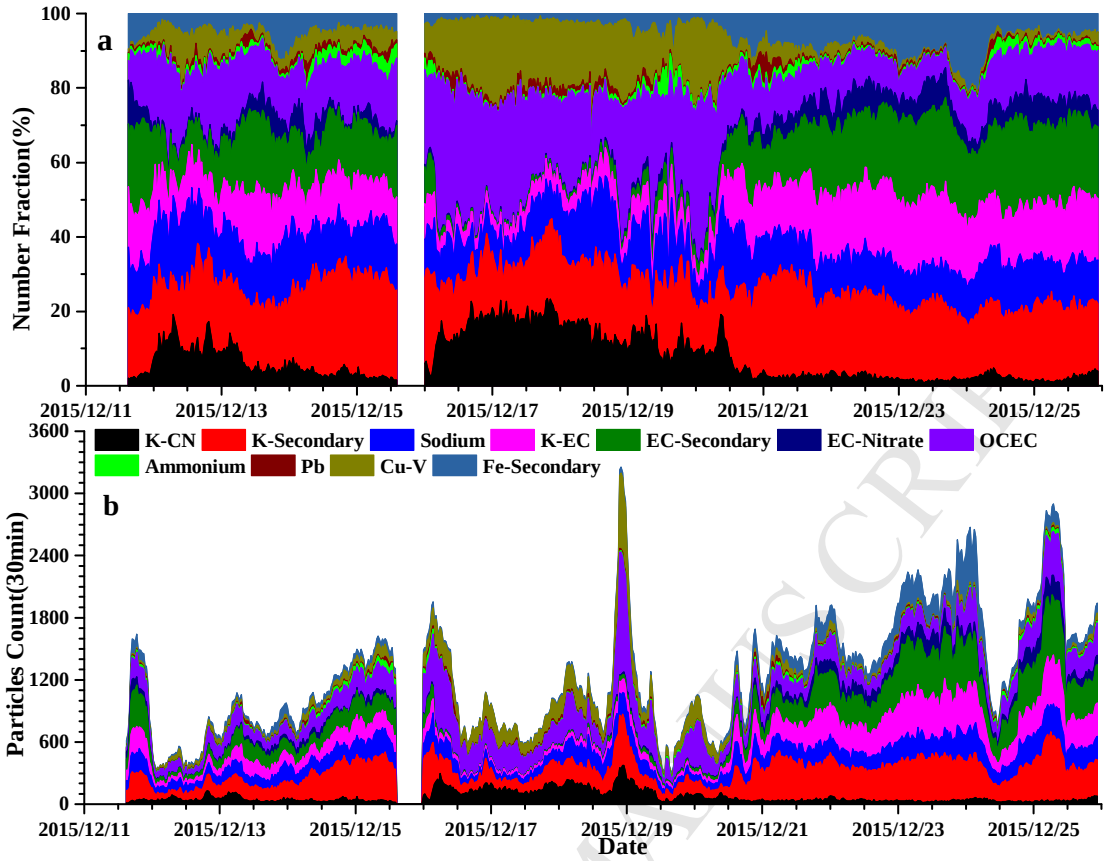

Figure 6. Temporal variations and the number fraction of the single particle types during the observation period

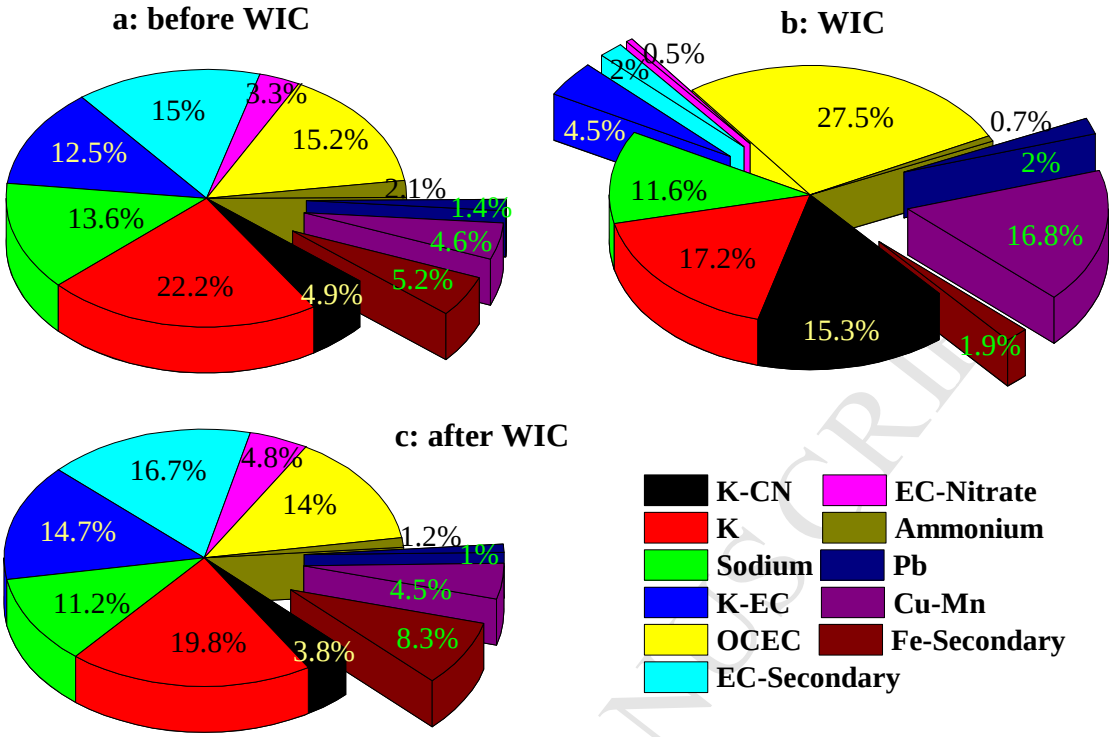

Figure 7. The fraction numbers of single particle types during different observation stages

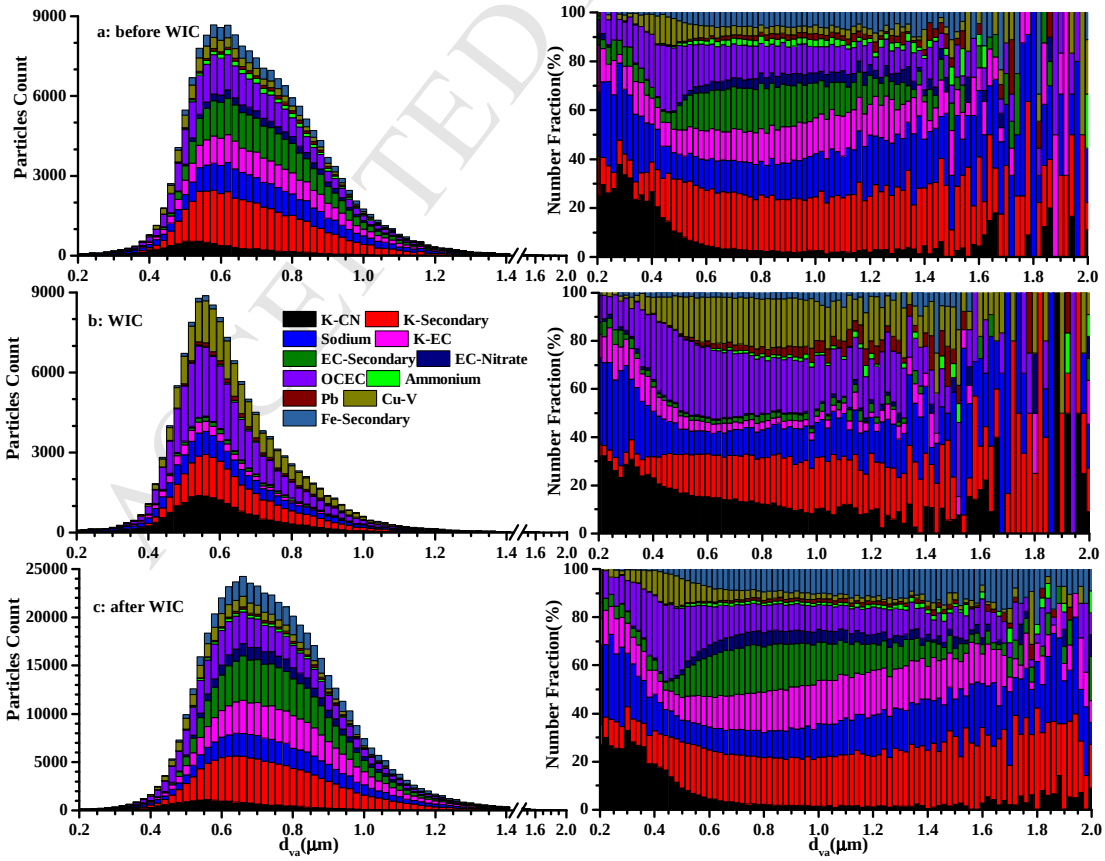

Figure 8 Size distribution and number fractions of single particle types during different observation stages

Highlights

1. The concentrations of $PM_{2.5}$, PM_{10}, NO_2, and CO were decreased by 31.2-62.1 % during the WIC.

2. SPAMS was used to characterize more than 877,397 single particles.

3. Signals from 23$[Na]^+$ were uniformly observed among 11 types of particles.

4. The proportions of K-CN, OCEC, and Cu-V particles increased significantly during the WIC.